Check for updates

Stabilisation and reactivity studies of donor-base ligand-supported gallium-phosphides with stronger binding energy: a theoretical approach†

Maria Francis [ID] and Sudipta Roy [ID] *

Gallium phosphide is a three-dimensional polymeric material of the hetero-diatomic GaP unit, which has a wurtzite type structure, and captivating application as a light emitting diode (LED). As a result, there is a constant search for suitable precursors to synthesise GaP-based materials. However, the corresponding monomeric species is exotic in nature due to the expected Ga≡P multiple bond. Herein, we report on the theoretical studies of stability, chemical bonding, and reactivity of the monomeric gallium phosphides with two donor base ligands having tuneable binding energies. We have performed detailed investigations using density functional theory at three different levels (BP86/def2-TZVPP, B3LYP/def2-TZVPP, M06-2X/def2-TZVPP), QTAIM and EDA-NOCV (BP86-D3(BJ)/TZ2P, M06-2X/TZ2P) to analyse various ligand-stabilised GaP monomers, which revealed the synthetic viability of such species in the presence of stable singlet carbenes, *e.g.*, cAAC, and NHC as ligands [cAAC = cyclic alkyl(amino) carbene, NHC = N-heterocyclic carbene] due to the larger bond dissociation energy compared to a phosphine ligand (PMe₃). The calculated bond dissociation energies between a pair of ligands and the monomeric GaP unit are found to be in the range of 87 to 137 kcal mol⁻¹, predicting their possible syntheses in the laboratory. Further, the reactivity of such species with metal carbonyls [Fe(CO)₄, and Ni(CO)₃] have been theoretically investigated.

Introduction

Gallium phosphide (GaP) is widely used in semiconductor containing devices, like long-wavelength detectors and semi-conductor lasers, light emitting diodes (LEDs), and as a host material for diluted magnetic semiconductors, because of its low cost, excellent optical properties, and good performance.[1–10] Due to its extensive use in electroluminescent devices, gallium phosphide (GaP), having an indirect band gap with a zinc blende (ZnS) structure (wurtzite/w-BN), is one of the very important group III–V semiconductors with the highest industrial importance, and used in MOCVD (MOCVD = metal organic chemical vapour deposition) processes.[11–14] By virtue of the 2.26 eV band gap, GaP emits at 555 nm, which makes it not just a semiconducting material, but also a green light emitting LED. The advantageous spectral range of GaP is found to be between 570 nm to 11 μm.[15] Moreover, GaP has the highest refractive index of 3.1 in the visible region. This helps to remove a few challenges in designing optical elements, and fast lens. Another crucial property of GaP is the mechanical durability, and chemical resistivity compared to other materials in the same

family, leading to useful optical materials that are subjected to mechanical stress, extreme weather, or abrasive dust.[16–19] Although, GaP is a polymeric material in the solid-state,[15] from the view point of main group chemists we were curious about the chemical bonding, and stability of the corresponding monomeric species, since such combination of heavier elements might lead to an exotic bonding scenario due to the poor overlap of their respective diffused valence orbitals.[20] The presence of internal nodes in the more diffused valence orbitals make the heavier main group elements unusual when compared to their lighter analgues.[20] The Pauli repulsion energy, and the London dispersion forces play a crucial role in their chemical bonding for possible isolation in the laboratory. In the recent times, the chemistry of molecules having bonds between group 13, and 15 atoms has drawn extensive attention. However, due to the immense synthetic challenges to stabilize such species, there are only a few experimental reports on GaP single and multiple bonded compounds.[21–28] The representative Ga–P containing species, which have been isolated in the laboratory by various research groups are shown in Fig. 1. More than two decades ago, Hoffmann *et al.* have theoretically studied GaP multiple bonds showing Ga≡P triple bond possessing the bond dissociation energy of 101 kcal mol⁻¹ at MP2/6-311++G(d,p) level of theory, while the corresponding values of GaP single and double bonds were found to be 62, and 89 kcal mol⁻¹, respectively.[28b] Very recently, Schulz group has

Department of Chemistry, Indian Institute of Science Education and Research (IISER) Tirupati, Tirupati 517507, India. E-mail: roy.sudipta@iisertirupati.ac.in

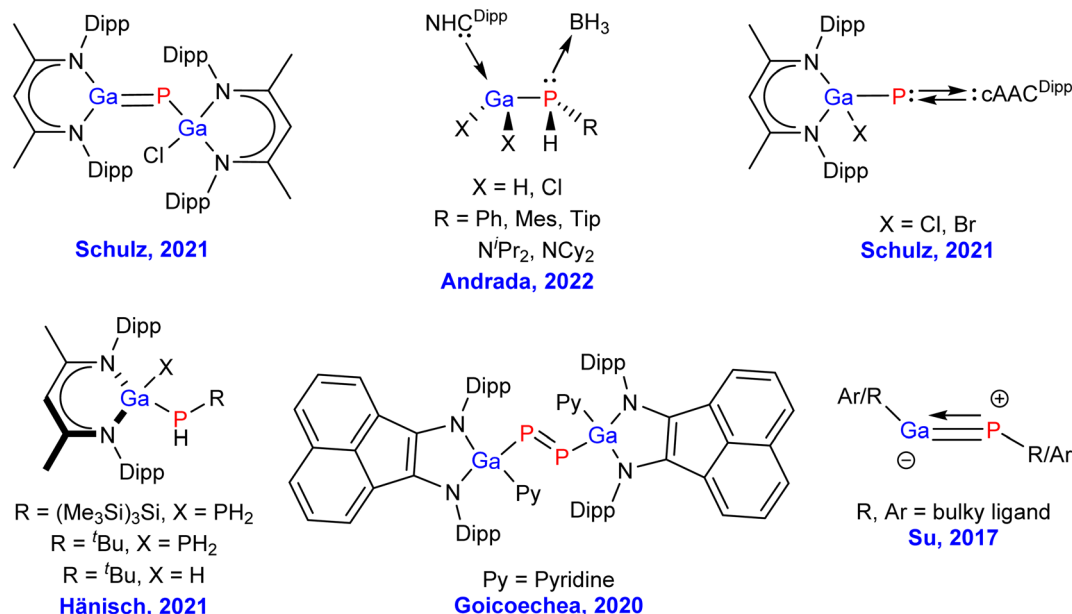† Electronic supplementary information (ESI) available. See DOI: https://doi.org/10.1039/d2ra06001a

Fig. 1 Representative GaP containing species isolated in the laboratory.

synthesized gallophosphene L(Cl)GaPGaL (L = HC[C-(Me) N(2,6-^{i}Pr$_2$C$_6$H$_3$)]$_2$), which can be used for heteroallyl cation generation, CO$_2$ storage, and C(sp^3)–H bond activation.[22] The same group has isolated cAAC^{Dipp} = P–Ga(Cl)L species (Fig. 1, top right).[27] Ming–Der Su and co-workers have theoretically predicted the triply bonded Ga≡P species using covalently bonded sterically bulky ligands (Fig. 1).[29] However, the GaP moiety, stabilised by neutral, donor base ligands, such as, carbenes and phosphines could not be isolated in the laboratory so far.

Herein, we report on the detailed theoretical studies on stability, chemical bonding, and reactivity of two donor base ligands-supported monomeric gallium phosphides with general formula (L)GaP(L′) [L,L′ = neutral donor base ligand, *e.g.*, carbene and phosphine; L,L′ = cAAC^{Me} (**1**); L = cAAC^{Me}, L′ = NHC^{Me} (**2**); L = cAAC^{Me}, L′ = PMe$_3$ (**3**); L = NHC^{Me}, L′ = cAAC^{Me} (**4**); L = NHC^{Me}, L′ = PMe$_3$ (**5**); L,L′ = NHC^{Me} (**6**); L,L′ = NHC^{DMP} (**6′**) (DMP = 2,6-dimethylphenyl); L,L′ = PMe$_3$ (**7**)] (Scheme 1) by using density functional theory (DFT) at three different levels (BP86/def2-TZVPP, B3LYP/def2-TZVPP, and M06-2X/def2-TZVPP), QTAIM,
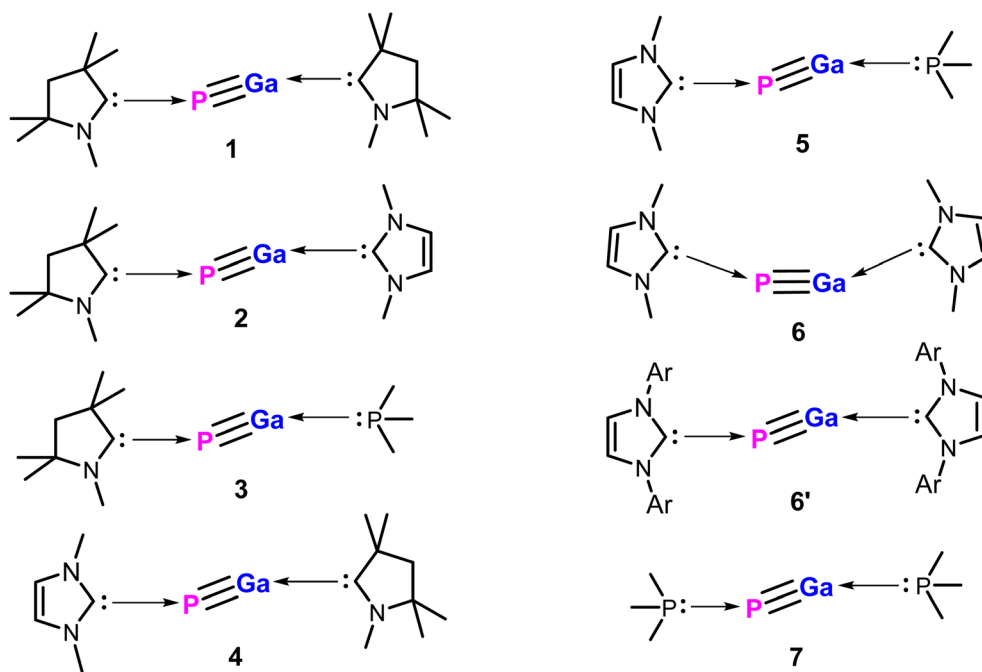
Scheme 1 Apparent structures of compounds **1–7** containing a pair of donor base ligands. Ar = 2,6-Dimethylphenyl.

and energy decomposition analysis coupled with natural orbital for chemical valence (EDA-NOCV) (at BP86-D3(BJ)/TZ2P, and M06-2X/TZ2P) methods to demonstrate the synthetic viability of such species.[30] These species, once isolated in the laboratory with neutral ligands, and sizeable bond dissociation energies, could be the promising precursors for GaP-based materials. Furthermore, we have studied the stability, and bonding of the corresponding metal carbonyl complexes of compound **1** with general formula $(cAAC)_2GaP-MCO_n$ [M = Fe; n = 4 (**8**), M = Ni; n = 3 (**9**)].

Very often, the EDA-NOCV method has been proven to be a significant tool for predicting the stability, and synthetic viability of exotic species.[31] In this context, it is worth mentioning that recently, our group has reported the successful syntheses of carbene-supported phosphinidene-chloroterylenes[31a] following our previous theoretical prediction of such elusive species.[32]

The role played by the ligands employed in stabilizing such exotic species are often found to be pivotal. These elusive species have been stabilised with success either by donor-base ligands or by sterically bulky ligands. Superior candidates for stabilizing these transient molecules are in general, the donor ligands, like phosphines, NHCs (N-heterocyclic carbenes), and cAACs (cyclic alkyl(amino) carbenes).[33] During the past two decades, using carbenes as ligands have had a tremendous impact on synthetic accomplishments of various apparently elusive species.[33–35] A significant number of these carbene containing species are now used for various applications in material chemistry, catalysis, *etc.*[36]

Computational methods

The geometry optimisations and frequency calculations of compounds **1–7** with general formula L-PGa-L′ [L,L′ = cAAC^{Me} (**1**); L = cAAC^{Me}, L′ = NHC^{Me} (**2**); L = cAAC^{Me}, L′ = PMe$_3$ (**3**); L = NHC^{Me}, L′ = cAAC^{Me} (**4**); L = NHC^{Me}, L′ = PMe$_3$ (**5**); L,L′ = NHC^{Me} (**6**); L,L′ = NHC^{DMP} (DMP = 2,6-dimethylphenyl) (**6′**); L,L′ = PMe$_3$ (**7**)] and **8–9** with general formula $(cAAC)_2GaP$-MCO$_n$ [M = Fe; n = 4 (**8**), M = Ni; n = 3 (**9**)] were performed at BP86/def2-TZVPP,[37] B3LYP/def2-TZVPP[37a,38] (hybrid functional), and M06-2X/def2-TZVPP (meta-hybrid functional)[39] levels using Gaussian 16.[40] BP86 (ref. 37) is composed of generalized gradient approximation (GGA) functional with Becke 1988[37a] exchange functional, and Perdew 86[37b] correlation functional. BP86, and B3LYP[37a,38] consist of Becke function in common with P86 correlation functional and 3LYP (Lee–Yang–Parr) exchange-correlation function, respectively. B3LYP is a hybrid functional, which is typically faster than the majority of Post–Hartree–Fock approaches and produces comparable outcomes. It covers Hartree–Fock exchange, local exchange, gradient exchange correction, local correlation, and gradient correlation correction involving different mixing parameters:

$$E_{XC} = 0.2 \times E_X(HF) + 0.8 \times E_X(LSDA) + 0.72 \\ \times DE_X(B88) + 0.81 \times E_C(LYP) + 0.19 \times E_C(VWN) \quad (1)$$

HF = Hartree–Hock, LSDA = Local Spin Density Approximation, E_X(B88) = Becke exchange functional, VWN = Vosko,

Wilk, and Nusair 1980 correlation functional, E_C(LYP) = Lee–Yang–Parr exchange-correlation function. M06-2X[39] is a functional with double the amount of the nonlocal exchange 2×, parameterized exclusively for main group elements. It is a combination of four meta-GGA, and hybrid meta-GGA functionals with 54% HF exchange, which are constructed by empirically fitting their parameters and constrained to a uniform electron gas. It is highly parameterized with approximate exchange-correlation energy functionals. M06-2X functional is quite useful for the kinetics, thermochemistry, noncovalent interactions, electronic excitation energies to valence, and Rydberg states for main-group compounds.

All of our calculations were performed including dispersion corrections. The absence of imaginary frequency indicated that the optimised molecules are at the minima of the potential energy surfaces. The Wiberg bond indices (WBI),[41] occupation numbers (ON), partial charges (q) on the atoms, and natural bond orbitals have all been evaluated using the NBO 6.0 programme on the above mentioned three levels.[42] Wavefunction generation were performed using the BP86/def2-TZVPP and M06-2X/def2-TZVPP levels of theory and basis set. Laplacian of electron density were generated using AIMALL software package.[43] Using the ADF 2020.102 software package, energy decomposition analysis (EDA)[30b] coupled with natural orbitals for the chemical valence (NOCV)[30c,d] computations were carried out on pre-optimised geometries at the BP86-D3(BJ)/def2-TZVPP level. EDA-NOCV were carried out for selected molecules in M06-2X/def2-TZV2P including Grimme dispersion. The EDA-NOCV approach entails the decomposition of the intrinsic interaction energy (ΔE_{int}) between the two fragments into the following four energy components:

$$\Delta E_{int} = \Delta E_{elstat} + \Delta E_{Pauli} + \Delta E_{orb} + \Delta E_{disp} \quad (2)$$

The interaction energy, ΔE_{int}, is the actual energy change that occurs when the geometrically deformed fragments unite to form the overall complex. The term ΔE_{elstat}, usually attractive, refers to the classical electrostatic interaction between the unperturbed charge distributions of the fragments in the geometry. The Pauli-repulsion, ΔE_{Pauli}, between these fragments consists of destabilising interactions between occupied orbitals and is responsible for steric repulsion. The orbital interaction, ΔE_{orb}, between these fragments account for bond pair formation, charge transfer (empty/occupied orbital mixing between different fragments), and polarisation (empty/occupied orbital mixing on one fragment due to the presence of another fragment). Finally, the ΔE_{disp} term considers the attractive dispersion interactions.

The NOCV approach identifies the orbitals of the components A and B that contribute the most to the formation of the bond A–B. Deformation density ($\Delta\rho(r)$) can be defined as the between the densities of the fragments before and after bond formation which can be expressed as

$$\Delta\rho(r) = \sum_k v_k \left[-\psi_{-k}^2(r) + \psi_{-k}^2(r) \right] = \sum_k \Delta\rho_k(r) \quad (3)$$

where ψ_{-k} and ψ_k are the pairs of eigen functions and v_k is the eigen value. The eigen function and eigen value is obtained

from the diagonalization of deformation density matrix. In a similar manner the total orbital interaction ΔE_{orb} can be defined from the pairwise orbital interaction energies, $\Delta E_{\mathrm{orb}}^{\mathrm{k}}$

$$\Delta E_{\mathrm{orb}} = \sum_{\mathrm{k}} v_{\mathrm{k}} \left[-F_{-\mathrm{k},-\mathrm{k}}^{\mathrm{TS}} + F_{-\mathrm{k},-\mathrm{k}}^{\mathrm{TS}} \right] = \sum_{\mathrm{k}} \Delta E_{\mathrm{orb}}^{\mathrm{k}} \qquad (4)$$

The terms $F_{-\mathrm{k},-\mathrm{k}}^{\mathrm{TS}}$ and $F_{-\mathrm{k},-\mathrm{k}}^{\mathrm{TS}}$ are diagonal transition-state (TS) Kohn–Sham matrix elements corresponding to NOCVs with the eigenvalues $-v_{\mathrm{k}}$ and v_{k}, respectively.

Method validation

We performed our studies in pure GGA (BP86),[44] hybrid GGA (B3LYP), and meta-GGA (M06-2X) functionals. The structural parameters of equilibrium geometries for compounds **1–7** were found to be slightly different in three level of theories (see ESI†). The singlet-triplet energy gaps of **1–7** with M06-2X functional were found to be in between to those values calculated with B3LYP, and M06-2X functionals. The bond dissociation energies (BDE) of **1–6′** were found to be close to each other with M06-2X, and B3LYP functionals. However, the lowest BDE values were obtained with M06-2X functional.

Results and discussion

We initiated our studies with structural optimizations of all the proposed molecules, **1–7** at BP86/def2-TZVPP,[37] B3LYP/def2-TZVPP,[37a,38] and M06-2X/def2-TZV2P[39] levels of theory in both singlet and triplet states. For all molecules (**1–7**), it was found that the singlet states are lower in energy compared to the
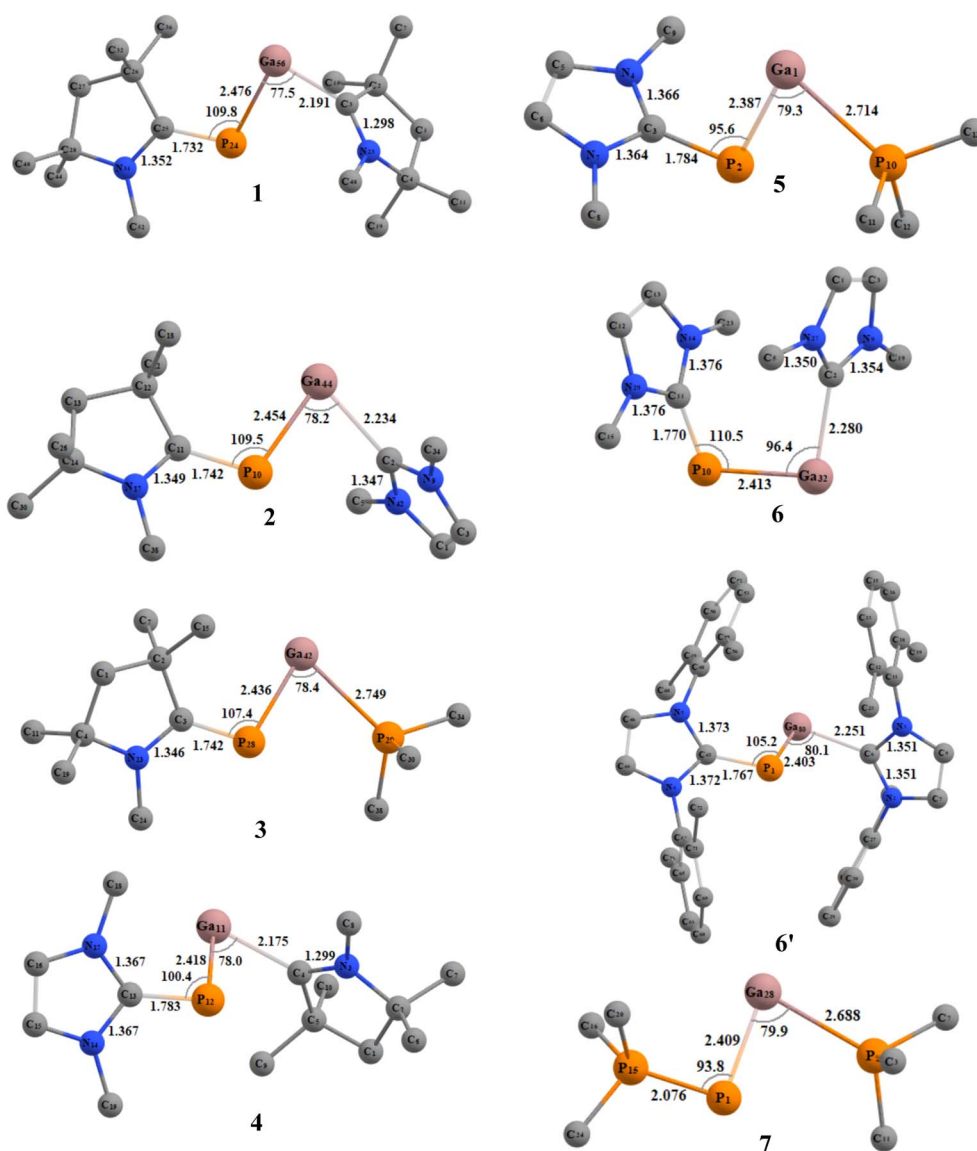

Fig. 2 Optimized geometries of compounds **1** to **7** in singlet ground state with L,L′ = cAAC$^{\mathrm{Me}}$ (**1**); L = cAAC$^{\mathrm{Me}}$, L′ = NHC$^{\mathrm{Me}}$ (**2**); L = cAAC$^{\mathrm{Me}}$, L′ = PMe$_3$ (**3**); L = NHC$^{\mathrm{Me}}$, L′ = cAAC$^{\mathrm{Me}}$ (**4**); L = NHC$^{\mathrm{Me}}$, L′ = PMe$_3$ (**5**); L,L′ = NHC$^{\mathrm{Me}}$ (**6**); L,L′ = NHC$^{\mathrm{DMP}}$ (DMP = 2,6-dimethylphenyl) (**6′**); L,L′ = PMe$_3$ (**7**) at M06-2X/def2-TZVPP level of theory.
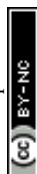
triplet states by 12.09–35.33 kcal mol^{-1} (Table S1†), and thus the singlet states are considered to be the ground states for **1–7** (Fig. 2). The absence of imaginary frequencies promises the minima on the potential energy surface in each case.

The PGa moiety in compounds **1**, **6**, and **7** is flanked by cAAC (cyclic alkyl(amino) carbene), NHC (N-heterocyclic carbene), and PMe$_3$ ligands; whereas in the remaining compounds, the ligands at P atom are either cAAC (**2**, **3**) or NHC (**4**, **5**), and at Ga there are different types of donor ligands, such as, cAAC, NHC and PMe$_3$. The extent of σ-donation and π-backdonation properties of the ligands employed in this study decide the final bonding of the compounds **1–7**. The optimised geometries shown in Fig. 2 shows that in all the compound except **6**, the ligands are arranged in *trans* fashion with respect to the PGa moiety, whereas in **6**, the ligands are arranged in a *cis* manner. The unusual *cis* geometry of compound **6** insisted us to change the *N*-substitution of the NHC ligand to a bulkier group, *viz.*, the 2,6-dimethyl phenyl (DMP) group (**6′**). The profound effect of the bulkier groups at N atoms of NHC was reflected in the changed orientation of the ligands from *cis* to a more favoured *trans* geometry. The energy difference between the singlet and triplet states of **6′** was found to be 26.07 kcal mol^{-1} (at BP86-D3(BJ)/def2-TZVPP), which is 1.31 kcal mol^{-1} higher than **6**. For compounds **1–7**, the calculated bond parameters at three different levels were found to be comparable (Tables S5 and S6†). The calculated C$_{cAAC}$–P bond length (at BP86-D3(BJ)/def2-TZVPP) was found to be approximately the same as 1.75 Å, when the P bonded ligand was cAAC (1.732, 1.742, and 1.742 Å,

respectively for the compounds **1**, **2**, and **3**), which are in well agreement with the laboratory isolated chlorophosphinidene (cAAC)P–Cl (1.7513 (15) Å),[45] and the related computationally studied molecules.[30] The calculated C$_{cAAC}$–P bond lengths were found to be similar when calculated at B3LYP/def2-TZVPP, and M06-2X/def2-TZVPP levels (Table S5†). When the P bonded ligand changes from cAAC to NHC (in **4–6**), a significant elongation was observed in the C$_{NHC}$–P bond lengths (1.783–1.784 Å in compounds **4–5**, and 1.770 (1.767) Å in compound **6** (**6′**)) (Table S5†), which is longer than the C$_{NHC}$–P bond found in the isolated NHC-stabilized diphosphorous (1.7504 (17), 1.754 (3) Å).[47] However, the C$_{NHC}$–P bond length falls in between a C–P single bond (1.839 (5) Å),[46] and double bonds of non-conjugated phosphaalkenes (1.65–1.67 Å).[47] The C$_{NHC}$–P bond length in **6′** with bulkier NHCs remained almost unchanged, but slight shortening of the bond length of P–Ga (0.01 Å), and Ga–C$_{NHC}$ (0.029 Å) were observed when compared to the same in compound **6** with smaller substitutions at the N atoms. Similarly, there was also reduction of bond angles observed at P and Ga centres. The C$_{NHC}$–P–Ga and P–Ga–C$_{NHC}$ bond angles were found to be 105.2° and 80.1°, respectively (at M06-2X/def2-TZVPP). The Ga–C$_{cAAC}$ bond lengths in compounds **1**, and **4** were found to be 2.191, and 2.175 Å, respectively, which are considerably longer than the same observed in the isolated cAAC-stabilised Ga radicals based on amidinate scaffolds (1.9342 (17) Å).[48] The EDA-NOCV studies conducted on C$_{cAAC}$–Ga bond by the authors[48] on the cAAC stabilised Ga radicals based on amidinate scaffolds suggests that the bond between

Table 1 NBO results of the compounds cAAC–P–Ga–cAAC^{Me} (**1**), cAAC–P–Ga–NHC^{Me} (**2**), cAAC–P–Ga–PMe$_3$ (**3**), NHC^{Me}–P–Ga–cAAC^{Me} (**4**), NHC^{Me}–P–Ga–PMe$_3$ (**5**), NHC^{Me}–P–Ga–NHC^{Me} (**6**) and PMe$_3$–P–Ga–PMe$_3$ (**7**) at the BP86-D3(BJ)/def2-TZVPP level of theory. Occupation number (ON), polarization and hybridization of the L–P, P–Ga and Ga–L′ bonds

Compound	Bond	ON	Polarization and hybridization (%)		WBI	q P	Ga
1	C25–P24	1.97	P: 34.0 s(19.0), p(80.2)	C: 66.0 s(39.7), p(60.0)	1.47	−0.27	0.34
		1.87	P: 60.4 s(0.1), p(99.5)	C: 39.6 s(0.0), p(99.8)			
	P24–Ga56	1.80	P: 76.1 s(15.4), p(84.0)	Ga: 23.9 s(10.6), p(89.1)	0.81		
	Ga56–C3	1.91	C: 86.1 s(39.6), p(60.3)	Ga: 13.9 s(8.3), p(91.3)	0.69		
2	P10–C11	1.86	P: 60.3 s(0.1), p(99.5)	C: 39.7 s(0.0), p(99.8)	1.47	−0.33	0.22
		1.97	P: 34.0 s(19.7), p(79.6)	C: 66.0 s(39.9), p(59.7)			
	P10–Ga44	1.86	P: 77.1% s(15.7), p(83.7)	Ga: 22.9% s(8.5), p(91.1)	0.83		
	Ga44–C2	1.92	C: 86.4% s(41.8), p(58.2)	Ga: 13.6% s(5.33), p(94.1)	0.52		
3	P28–C3	1.97	P: 34.5 s(20.5), p(78.8)	C:65.5 s(39.8), p(59.9)	1.47	−0.40	0.21
		1.86	P: 60.8 s(0.0), p(99.5)	C: 39.2 s(0.0), p(99.8)			
	P28–Ga42	1.89	P: 78.6 s(14.8), p(84.7)	Ga: 21.4 S(7.2), p(92.6)	0.84		
	Ga42–P29	1.90	P: 87.8 s(30.0), p(69.9)	Ga: 12.2 S(2.6), p(96.9)	0.41		
4	P12–C13	1.97	P: 32.4 s(14.8), p(84.3)	C: 67.6 s(43.6), p(56.1)	1.22	−0.44	0.28
	P12–Ga11	1.80	P: 82.7 s(10.8), p(88.7)	Ga: 17.3 s(5.1), p(94.4)	0.89		
	Ga11–C4	1.90	C: 86.0 s(39.4), p(60.5)	Ga: 14.0 s(8.0), p(91.4)	0.66		
5	P2–C3	1.97	P: 32.9 s(15.5), p(83.6)	C: 67.1 s(43.6), p(56.1)	1.23	−0.54	0.17
	P2–Ga1	1.85	P: 84.8 s(3.6), p(96.6)	Ga: 15.2 s(2.0), p(97.6)	0.94		
	Ga1–P10	1.90	P: 87.9 s(30.4), p(69.6)	Ga: 12.1 s(2.8), p(96.7)	0.42		
6	C11–P10	1.97	P: 32.5 s(15.9), p(83.3)	C: 67.5 s(44.5), p(55.2)	1.28	−0.41	0.23
	P10–Ga32	1.81	P: 85.2 s(3.2), p(96.3)	Ga: 14.8 s(2.0), p(97.5)	0.93		
	Ga32–C2	1.93	C: 87.2 s(41.6), p(58.4)	Ga: 12.8 s(5.2), p(94.4)	0.48		
7	P15–P1	1.97	P15: 59.1 s(32.2), p(67.23)	P1: 40.9 s(13.4), p(85.4)	1.26	−0.82	0.16
	P1–Ga28	1.85	P: 79.2 s(13.1), p(85.9)	Ga: 20.8 s(7.5), p(92.4)	0.92		
	Ga28–P2	1.91	Ga: 13.1 s(3.4), p(96.2)	P: 86.9 s(30.5), p(69.5)	0.45		

Ga and the cAAC is covalent, and not a coordinate bond. From this, we may suggest that the C_{cAAC}–Ga bond might not be a covalent bond, because it is slightly elongated than the experimentally observed C_{cAAC}–Ga bond in the cAAC-stabilised Ga radicals.[49] When the Ga-bonded ligand is NHC, the bond length is 2.234, and 2.280 Å for **2**, and **6** admitting with NHC-stabilised Ga–P compounds, like the monomeric [(IMes)GaEt$_2$-P(H)Si^{t}BuPh$_2$] (2.1254 (7) Å),[49] but shorter than the NHC-stabilised silylphosphogallanes (2.059 (2), 2.077 (3)–2.087 (3) Å).[50] The bond length of P–Ga in **6** is found to be approximately 2.40 Å (Fig. 2). The group of Ming-Der Su theoretically studied the stability of the GaP moiety using various ligands, such as, F, OH, H, CH$_3$, SiH$_3$, SiMe(Si^{t}But$_3$)$_2$, Si^{i}PrDis$_2$, Tbt (C$_6$H$_2$-2,4,6-{CH(SiMe$_3$)$_2$}$_3$), and Ar* (C$_6$H$_3$-2,6-(C$_6$H$_2$-2,4,6-^{i}Pr$_3$)$_2$).[29] Their theoretical observations proved that the triply bonded Ga≡P could be effectively stabilised by employing bulkier, and stronger donating ligands. The observed triple bond length was in the range of 2.146–2.183 Å,[29] while the GaP bond distances

for a single and triple bonds are 2.328 and 2.067 Å, respectively, at MP2/6-311++G(d,p) level of theory.[28b] However, in our studies, when we tried stabilising the GaP moiety using carbenes, we could see considerable elongation of the bond length, which is conceding in the range of Ga–P single bond. The GaP bond length observed in the NHC-stabilised silylphosphogallanes is slightly shorter than the theoretically observed bond lengths (2.365 (6)–2.366 (6) Å, and 2.372 (1)–2.373 (1) Å).[50] When the Ga-bonded ligand is PMe$_3$, the bond between is found to be significantly higher than the GaP moiety. In compounds **3/5** the Ga–P$_{PMe3}$ bond lengths are 2.749/2.714 Å. These bond lengths typically fall in the range of GaP adducts (2.582 and 2.720 Å).[51] We have calculated the bond dissociation energies (BDE) for the P–Ga bond at three different levels of theory (BP86/def2-TZVPP, B3LYP/def2-TZVPP, and M06-2X/def2-TZVPP). The highest BDE is overserved for compound **1** (125.38 kcal mol^{-1} (with M06-2X), 137.09 kcal mol^{-1} (with BP86), and 128.86 kcal mol^{-1} (with B3LPY). The least BDE is observed for the compound **7**
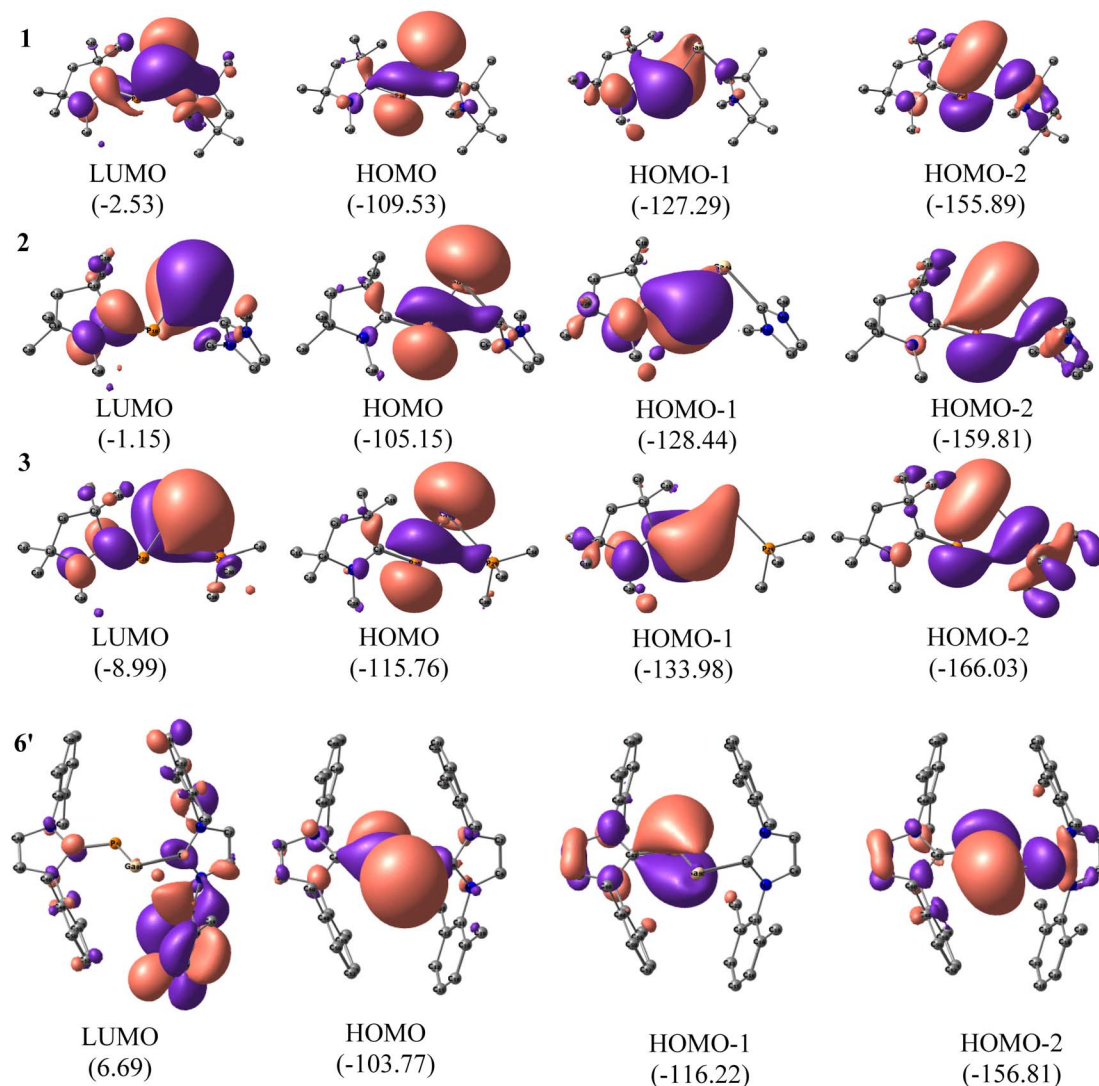

Fig. 3 The LUMO, HOMO, HOMO−1, and HOMO−2 of cAAC–P–Ga–cAAC^{Me} (**1**), cAAC–P–Ga–NHC^{Me} (**2**), and cAAC–P–Ga–PMe$_3$ (**3**) and **6′** with L,L′ = NHC^{DMP} at M06-2X/def2-TZVPP level of theory. The values in the parentheses are the energies of the orbitals in kcal mol^{-1}.

(87.644 kcal mol^{-1} (with M06-2X), 93.96 kcal mol^{-1} (with BP86), 89.44 kcal mol^{-1} (with B3LPY). When P bonded ligand is cAAC (**1–3**), the BDE increases in the order **3** < **2** < **1**. When P bonded ligand is NHC (**4–6**), the BDE increases in the order **5** < **6** < **4**. Both the trends mentioned above concludes that when the ligand on Ga is cAAC, highest bonding energy is observed. The second highest BDE is observed when the ligand is NHC, and the least when the ligand is PMe$_3$. When Ga is bonded to cAAC (**1**, **4**) the highest BDE was observed for **1** (P bonded ligand is cAAC), and when Ga bonded ligand is NHC (**2**, **6**) the highest BDE was observed for **2** (P bonded ligand is cAAC). In all the cases we observed the same trend. It follows the same trend as the electron donating and accepting nature of the ligands (cAAC > NHC > PMe$_3$). The σ-donating and π-accepting nature of cAAC ligands make the bond stronger, and thus the highest BDE is observed. The calculations performed at BP86 were highest compared to M06-2X, and B3LYP. The BDE computed at M06-2X, and B3LYP were found to be comparable for all the proposed molecules (Table S2†).

To understand the electronic structures of compounds **1–7**, we performed natural bond orbital (NBO) analyses[42] on the optimised coordinates at BP86-D3(BJ)/def2-TZVPP, B3LYP/def2-TZVPP, and M06-2X/def2-TZVPP levels of theory (Fig. 3 and S2†). The comparative results are included in the Fig. S2, and Tables 1, S23, S24.† When the P-bonded ligand is cAAC, the C$_{cAAC}$–P bond is having two occupancies, the first one polarized towards C$_{cAAC}$ (∼66%), and the other is polarized towards P (∼60%). We could observe only one occupancy on the Ga side, which is polarized towards ligand (86–87%). This could be due to the larger size and more diffused orbitals, and internal nodes of Ga. The Wiberg bond index (WBI) of compounds **1–3** clearly indicates the bond between C$_{cAAC}$–P is double bond (1.47). WBI observed for the bond between Ga–P of GaP moiety (0.81–0.93), and the values predict a single bond between Ga and P (Table 1). The WBI decreases for the bond between Ga–L, when the ligand changes from cAAC, NHC, and PMe$_3$ irrespective of the ligands bonded to P. The same trend is followed by the ligand's π-accepting property. The HOMOs of compounds **1–7** are the lone pairs of electrons on P, and Ga, mixing with the σ-electron pair of Ga–P bond. The HOMO−1 is essentially the cAAC═P π bond, which is in conjugation with the lone pair of the electron of Ga-atom. The HOMO−2 contains the lone pair on P atom, and the overlap of orbitals with the adjacent Ga atom having some interaction with σ-orbital of Ga–L$'$ (Fig. 3). The P-atom possesses a negative charge, while the Ga-atom of compounds **1–7** are positively charged as expected from their electronegativity values (see Table 1).

R. F. W. Bader and his team created the quantum theory of atoms in molecules (QTAIM), which is based on quantum observables like the electron density $\rho(r)$, and second derivative of energy densities $\nabla^2\rho(r)$.[52] The optimised geometries of compounds **1–7** were used to compute the wavefunctions for the QTAIM analyses at the BP86/def2-TZVPP level of theory. It is observed that the bonds between L–P (0.161–0.129 a.u.), and Ga–L$'$ (0.201–0.138 a.u.) is having greater $\nabla^2\rho(r)$, when the L and L$'$ are cAAC and NHC. But when L$'$ is PMe$_3$, it is observed that the Laplacian of electron density decreases, and it is very close

Table 2 The EDA-NOCV analyses of L–PGa–L$'$ bonds of L–P–Ga–L$'$ complex [LL$'$ = cAAC^{Me} (**1**), L = cAAC^{Me}, L$'$ = NHC^{Me} (**2**), L = NHC^{Me}, L$'$ = cAAC^{Me} (**4**), L = NHC^{Me}, L$'$ = PMe$_3$ (**5**), L,L$'$ = NHC^{Me} (**6**)] using [ligands] and [P–Ga] in the electronic singlet (S) states as interacting fragments at the BP86-D3(BJ)/TZ2P level of theory. Energies are in kcal mol^{-1}

Energy	Interaction	[(cAAC)₂] (S) + [P–Ga] (S)	[(cAAC) (NHC)] (S) + [P–Ga] (S)	[(NHC) (cAAC)] (S) + [P–Ga] (S)	[(NHC) (PMe₃)] (S) + [P–Ga] (S)	[(NHC)₂] (S) + [P–Ga] (S)
Compound		1	2	4	5	6
ΔE_{int}		−161.1	−163.2	−141.4	−125.5	−130.6
ΔE_{Pauli}		528.0	545.7	413.0	368.5	448.1
$\Delta E_{disp}{}^a$		−19.3 (2.8%)	−17.5 (2.5%)	−18.4 (3.3%)	−16.1 (3.3%)	−14.1 (2.4%)
$\Delta E_{elstat}{}^a$		−345.1 (50.1%)	−344.2 (48.6%)	−283.6 (51.2%)	−248.5 (50.3)	−285.2 (49.3%)
$\Delta E_{orb}{}^a$		−324.7 (47.1%)	−347.2 (48.9%)	−252.5 (45.5%)	−229.5 (46.4%)	−279.3 (48.3%)
$\Delta E_{orb(1)}{}^b$	L → P-Ga ← L$'$ σ donation	−174.5 (53.7%)	−214.1 (61.7%)	−139.3 (55.2%)	−139.2 (60.6%)	−158.7 (56.8%)
$\Delta E_{orb(2)}{}^b$	L → P-Ga ← L$'$ σ donation	−24.4 (7.5)	−69.4 (20.0%)	−33.7 (13.4%)	23.9 (10.4%)	−31.8 (11.4%)
$\Delta E_{orb(3)}{}^b$	L ← P-Ga → L$'$ π backdonation	−58.8 (18.1)	−27.4 (7.9%)	−44.3 (17.5%)	33.5 (14.6%)	−50.5 (18.1%)
$\Delta E_{orb(4)}{}^b$	L ← P-Ga → L$'$ π backdonation	−43.4 (13.4)	−15.2 (4.4%)		13.3 (5.8%)	−21.2 (7.6%)
$\Delta E_{orb(rest)}$			−36.3 (10.4%)	−35.2 (13.9%)	19.6 (8.6%)	−17.1 (6.1%)

^{a} The values in the parentheses show the contribution to the total attractive interaction $\Delta E_{disp} + \Delta E_{elstat} + \Delta E_{orb}$. ^{b} The values in the parentheses show the contribution to the total orbital interaction ΔE_{orb}.
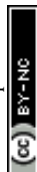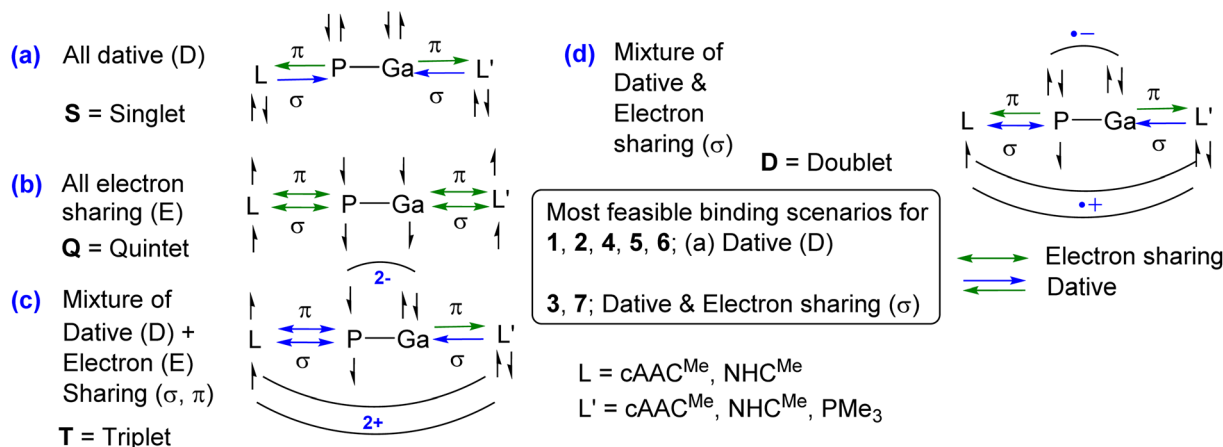
Scheme 2 Possible bonding scenarios of compounds **1–7** (also see Table S12†). (a) [L,L′] and [PGa] in neutral electronic singlet states forming a dative bond; (b) [L,L′] and [PGa] in neutral electronic quintet states forming four electron sharing/covalent bonds; (c) doubly charged [L,L′]$^{2+}$ and [PGa]$^{2-}$ fragments in triplet states forming σ electron sharing and π dative bonds; (d) singly charged [L,L′]$^{+}$ and [PAl]$^{-}$ fragments in doublet states forming both electron sharing and dative bonds.

to zero (0.032–0.040 a.u.). This reveals the better closed shell interaction when the ligands are carbenes. In the similar way, the values are close to zero (0.033–0.043 a.u.) for bonds between P and Ga of PGa moiety, implying a weaker closed shell interation. The $\rho(r)$ is observed for L–P is significantly higher compared to P–Ga and Ga–L′ bond. The bond's nature is measured by its ellipticity, ε. In the situation of single and triple bonds, where the bond is cylindrically symmetrical, ε is near to zero. Due to the asymmetrical distribution of electron density, perpendicular to the bond path, for a double bond, it is greater than zero. Ellipticity is observed the highest when the P bonded ligand is cAAC. The ligand cAAC being a good σ-donor and π-acceptor, this bond may have a partial double bond character.

We conducted energy decomposition analysis coupled with natural orbital for chemical valence (EDA-NOCV) at BP86-D3(BJ)/TZ2P and M06-2X/TZ2P level of theories to arrive at the best bonding description. EDA part was developed independently by Morokuma[30a] and by Ziegler and Rauk[30b]. Several decades later, NOCV analyses was introduced by M. Mitoraj, A. Michalak. The bonding scenarios have remained the same although the numerical values with BP86 and M06-2X functionals have varied slightly by 2–3% (Tables 2, 3 and Scheme 2) except compound 7. The ΔE_{int} of the species shown Tables 2 and 3 with two different functionals differ nearly by 20 kcal mol^{-1}. The values are smaller in M06-2X functionals. Frenking *et al.* have faced a similar problem with GGA functionals (BP86) with L_2E systems [E = BH, C, N$^+$; L = donor base ligands]. The authors have finally have shown that meta-GGA [M05-2X] are suitable for calculations of bond dissociation energies of those species.[46] The differences between these functionals have been discussed in the computational method.

Table 3 The EDA-NOCV analyses of L–PGa–L′ bonds of L–P–Ga–L′ complex [L,L′ = cAAC^{Me} (**1**), L = cAAC^{Me}, L′ = NHC^{Me} (**2**), L = NHC^{Me}, L′ = cAAC^{Me} (**4**), L,L′ = PMe$_3$ (**7**)] using [ligands] and [P–Ga] in the electronic singlet (S) states as interacting fragments at the M06-2X/TZ2P level of theory. Energies are in kcal mol^{-1}

Energy	Interaction	[(cAAC)$_2$] (S) + [P–Ga] (S)	[(cAAC) (NHC)] (S) + [P–Ga] (S)	[(NHC) (cAAC)] (S) + [P–Ga] (S)	[(PMe$_3$)$_2$] (S) + [P–Ga] (S)
Species		**1**	**2**	**4**	**7**
ΔE_{int}		−140.1	−136.3	−125.3	−96.9
ΔE_{Pauli}		553.9	508.3	401.1	291.3
ΔE_{disp}[a]		−0.38 (0.1%)	−0.27 (0.04%)	−0.3 (0.05%)	−0.14 (0.03%)
ΔE_{elstat}[a]		−360.5 (52%)	−331.3 (51.4%)	−292.1 (55.5%)	−195.7 (50.4%)
ΔE_{orb}[a]		−333.1 (48%)	−312.9 (48.5%)	−234.0 (44.45%)	−192.4 (49.6%)
$\Delta E_{orb(1)}$[b]	L → P–Ga ← L′ σ donation	−215.5 (64.7%)	−203.6 (65.1%)	−134.1 (57.3%)	−126.8 (65.9%)
$\Delta E_{orb(2)}$[b]	L → P–Ga ← L′ σ donation	−37.6 (11.3%)	−28.5 (9.1%)	−44.0 (18.8%)	29.3 (15.3%)
$\Delta E_{orb(3)}$[b]	L ← P–Ga → L′ π backdonation	−49.6 (14.9%)	−53.4 (17.1%)	−27.7 (11.8%)	18.8 (9.8%)
$\Delta E_{orb(4)}$[b]	L ← P–Ga → L′ π backdonation	−16.3 (4.9%)		−14.1 (6.0%)	13.1 (6.8%)
$\Delta E_{orb(rest)}$		−14.1 (4.2%)	−27.4 (8.7%)	−14.1 (6.0%)	4.4 (2.2%)

[a] The values in the parentheses show the contribution to the total attractive interaction $\Delta E_{disp} + \Delta E_{elstat} + \Delta E_{orb}$. [b] The values in parentheses show the contribution to the total orbital interaction ΔE_{orb}.

Each species was split into two fragments containing ligands $[(L)(L')]$ and the central PGa diatom in different spin and charged states. We have considered four different types of bonding interactions between the ligand pairs and PGa for the present studies. The first bonding possibility (Scheme 2a) is the interaction of neutral $[(L)(L')]$ and PGa fragments forming covalent dative bonds (single headed arrows) in their excited singlet states. The second bonding scenario (Scheme 2b) is the interaction of neutral $[(L)(L')]$ and PGa fragments forming four covalent electron sharing σ-bonds (double headed arrows) in their quintet states. The third bonding possibility (Scheme 2c) is the interaction of these fragments between doubly positive charged ligand and doubly negative charged PGa in their triplet electronic states (T), forming two electron sharing σ-bonds and two covalent π-dative bonds. The forth one (Scheme 2d) is the interaction of these fragments between singly positive charged
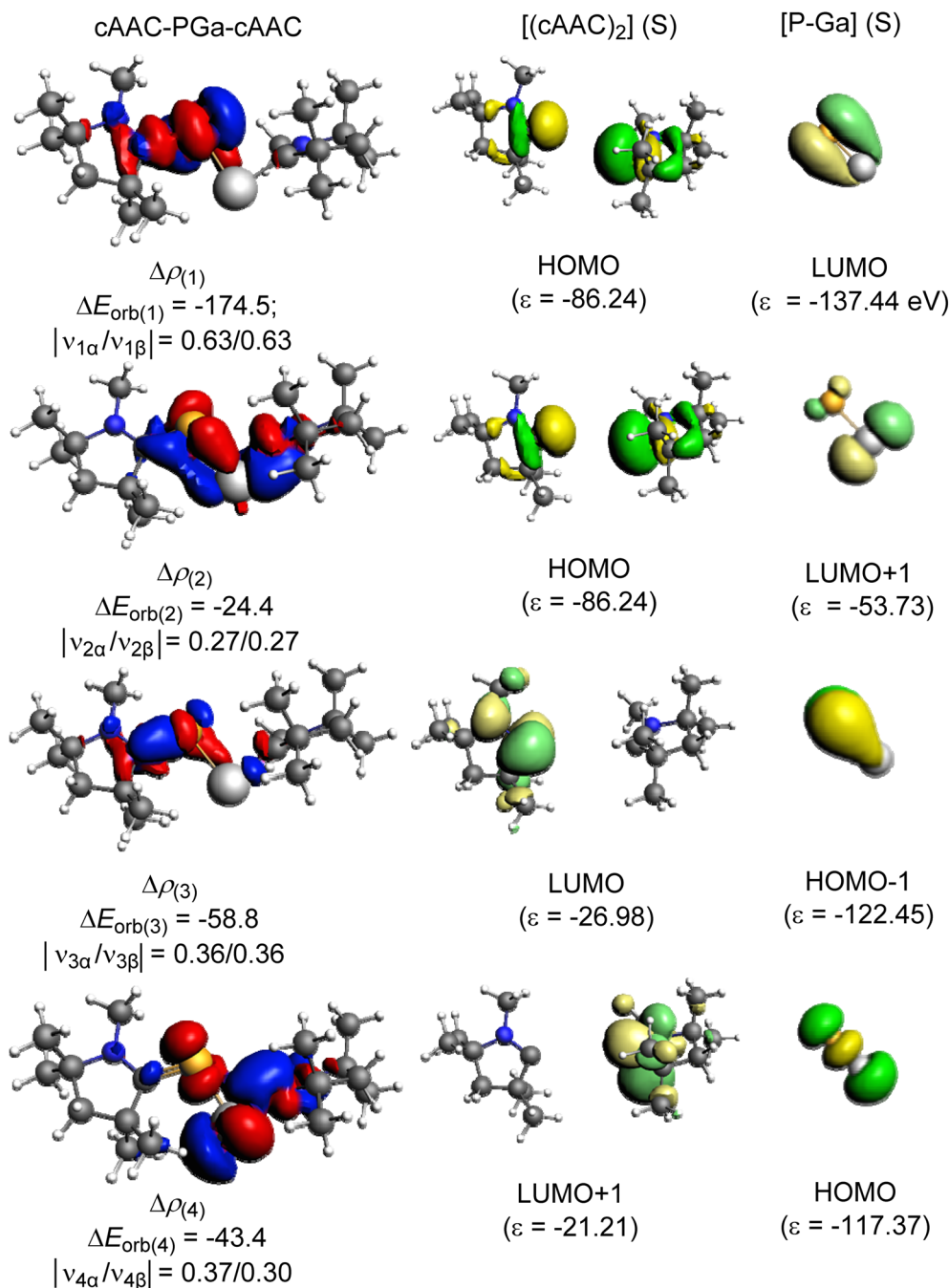
Fig. 4 The shape of the deformation densities $\Delta\rho_{(1)-(4)}$ that correspond to $\Delta E_{orb(1)-(4)}$, and the associated MOs of cAAC−P−Ga−cAAC (**1**) and the fragments orbitals of [(cAAC) (cAAC)] and [P−Ga] in the Singlet state (S) at the BP86-D3(BJ)/TZ2P level. Isosurface values are 0.003 au for $\Delta\rho_{(1)}$ and 0.001 au for $\Delta\rho_{(2-4)}$. The eigen values $|\nu_n|$ give the size of the charge migration in e. The direction of the charge flow of the deformation densities is red → blue. Energy values are in kcal mol^{-1}.
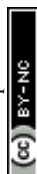
ligand and singly negative charged PGa in their doublet electronic states (D), forming one electron sharing σ-bonds and three covalent dative π-bonds. The summary of the bonding scenarios of **1–7** is shown in Scheme 2. Species **1**, **2**, **4–6** possess all four dative bonds (bonding scenario (a), Scheme 2) while **3** and **7** prefer bonding scenario (d) of Scheme 2 ([L,L′]$^+$ [PGa]$^−$).

EDA-NOCV results predicted the formation of dative bonds between ligands and the central PGa fragment. Out of the attractive energies, the electrostatic contribution (ΔE_{elstat} = 48.6–51.2%) is slightly more significant than the orbital contribution (ΔE_{orb} = 45.5–48.9%) (Table 2). The remaining contribution to the attractive force is contributed by dispersion energy which is small (ΔE_{disp} = 2.4–3.3%).

The pairwise breakdown of total orbital interactions (ΔE_{orb}) sheds more light on the nature of the bond. For compounds **1**, **2**, **5**, and **6**, the calculations show four relevant orbital contributions ($\Delta E_{orb(1-4)}$), whereas, for compounds **3**, **4**, and **7** the calculation predicted three significant orbital contributions ($\Delta E_{orb(1-3)}$). The first and the major orbital ($\Delta E_{orb(1)}$) contribution (53.7–61.7%) of the compounds **1**, **2**, **4**, **5**, and **6** involve the σ-donation from the filled orbital of [L,L′] to the vacant orbital of [PGa] fragment. The σ-donation happens from HOMO of [L,L′] fragment to LUMO of [PGa] in compounds **1**, **2**, and **5** and HOMO−1 of [L,L′] fragment to LUMO of [PGa] fragment in compounds **4**, and **6**. The second orbital contribution ($\Delta E_{orb(2)}$) describes another σ-donation, which is relatively weaker (7.5–20.0%) than the latter one. The third and fourth orbital contribution occurs due to the backdonation from [PGa] fragment to the [L,L′] fragment. In compound **1**, $\Delta E_{orb(3)}$ (18.1%) is due to the backdonation from LUMO of [PGa] to the HOMO−1 of [(cAAC)$_2$] and $\Delta E_{orb(4)}$ (13.4%) is due to the backdonation from LUMO+1 of [PGa] to the HOMO of [(cAAC)$_2$]. The contribution due to π-backdonation decreases considerably when the Ga-bonded ligand is NHC (**2**). $\Delta E_{orb(3)}$ and $\Delta E_{orb(4)}$ contributes 7.9 and 4.4%, and is due to the π-backdonation from HOMO of [PGa] to LUMO+3 of [(cAAC) (NHC)]. Only one orbital contribution, $\Delta E_{orb(3)}$, corresponding

to π-backdonation is observed in **4**, which is due to the π-backdonation from HOMO−1 of [PGa] to LUMO+1 of [(cAAC) (NHC)]. In compound **5** and **6**, $\Delta E_{orb(3)}$ contributes 14.6% and 18.1% to the total orbital contribution. π-backdonation happens from HOMO of [PGa] to LUMO of [(NHC) (PMe$_3$)] in **5**, and from HOMO of [PGa] to LUMO+2 of [(NHC)$_2$] in **6**. $\Delta E_{orb(4)}$ corresponds to a minor π backdonation (5.8% (**5**) and 7.6% (**6**)) from [PGa] to the ligand fragments. From the deformation plots (Fig. 4, 5, S12 and S19 in the ESI†), it is evident that the π-backdonation is more prominent from P to L (7.9–18.1%) rather than from Ga to L′ in **6**.

The unusual *cis*-geometry of compound **6** led to the N substitution being changed trans due to the bulkier groups on the N-atoms of NHC ligands of **6′**. One NHC ligand in **6**, which is formatting a dative bond with the Ga-atom, is expected to be electron deficient (δ^+), while in comparison, the other NHC ligand slightly electron rich (δ^-) (due to π-backdonation from P-atom to C$_{NHC}$ atom) leading to a dipolar π-stacking interaction between two five membered imidazole rings with a short C$_{NHC}$−C$_{NHC}$ bond distance of 3.097 Å (Fig. 5, right). The same is visible deformation densities (red and blue regions of two NHC C-atoms) of **6** (Fig. 5, left). This weak stabilisation interaction is overcome by the steric hindrance posed by the bulky groups on the N-atoms of the two NHC ligands leading to a *trans* geometry of **6′** (Fig. 2). For the compounds **3**, and **7** the best bonding possibility predicted by EDA-NOCV is the formation of both σ-electron sharing and dative bonds from the interaction of the singly charged doublet species of [L,L′]$^+$ and [PGa]$^−$. The contribution of electrostatic interaction energy (50.0%) between [L,L′] and [PGa]$^+$ is slightly higher than the orbital contribution (47.8%) towards the total attractive forces in compound **3**, whereas, these energies contribute equally in compound **7** (ΔE_{elstat} = 48.6%; ΔE_{orb} = 48.9%). The stabilisation due to dispersion energy (2.1% (**3**); 2.5% (**7**)) is small compared to the later energies discussed above. ΔE_{orb} can be further divided into three different pairwise interaction. The electron sharing bond formation between the ligand fragment and PGa is well
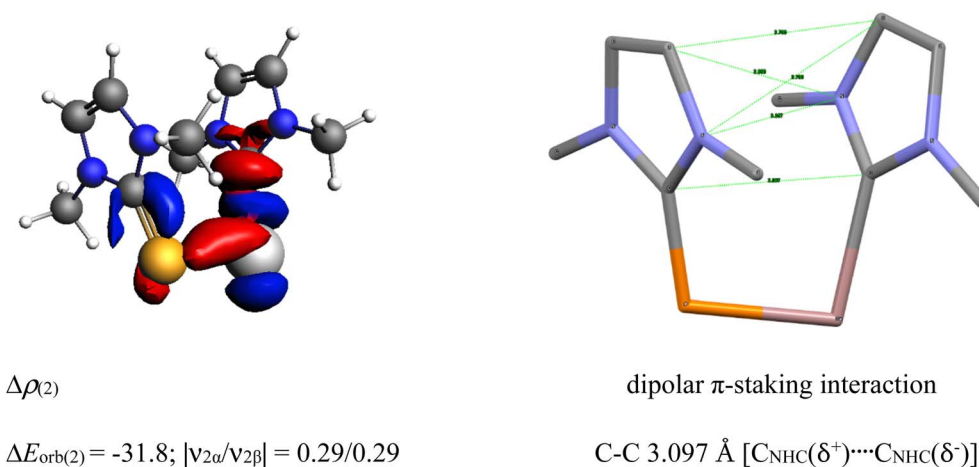

$\Delta\rho_{(2)}$

$\Delta E_{orb(2)}$ = -31.8; $|\nu_{2\alpha}/\nu_{2\beta}|$ = 0.29/0.29

dipolar π-staking interaction

C-C 3.097 Å [C$_{NHC}$(δ^+)····C$_{NHC}$(δ^-)]

Fig. 5 Selected deformation densities (left) and corresponding dipolar π-stacking interaction (right) of **6** with a short C−C bond distance of 3.097 Å [C$_{NHC}$(δ^+)...C$_{NHC}$(δ^-)].

described in ($\Delta E_{orb(1)}$) and this is the major contribution (67.3% (**3**); 66.0% (**7**) Table S13†) to the total orbital interaction.

$\Delta\rho_{(2)}$ dipolar π-stacking interaction

$$\Delta E_{orb(2)} = -31.8; |\nu_{2\alpha}/\nu_{2\beta}| = 0.29/0.29 \text{ C–C } 3.097 \text{ Å}$$
$$[C_{NHC}(\delta^+)...C_{NHC}(\delta^-)]$$

The dative out-of-phase σ-donation from HOMO of $[L,L']^+$ to $[PGa]^-$ in compound **3** and HOMO of $[L,L']^+$ to LUMO of $[PGa]^-$ in compound **7** is the second orbital term, $\Delta E_{orb(2)}$ (Fig. S10 and S13†). The most minuscule contribution (10.3% (**3**); 6.7% (**7**)) to the ΔE_{orb} is the π-backdonation from $[PGa]^-$ to $[L,L']^+$, which is depicted in $\Delta E_{orb(3)}$. π-backdonation is observed from

HOMO−1 of $[PGa]^-$ to LUMO+20 of $[L,L']^+$ and HOMO−1 of $[PGa]^-$ to LUMO+4 of $[L,L']^+$ in **3** and **7**, respectively.

Next, we tried to explore whether $(cAAC)_2PGa$ (**1**) can act as a ligand for the stabilisation of unsaturated metal-carbonyls having the general formulae $(cAAC)_2PGa$-$M(CO)_n$ [M = Fe (**8**), n = 4; Ni (**9**), n = 3] (Fig. 6, see ESI†). The optimized geometries of **8**–**9** have been displayed in Fig. 7.

The further theoretical analyses revealed that $(cAAC)_2PGa$-$Fe(CO)_4$ (**8**) may be stable and hence it may be isolated in the laboratory (see ESI†). The P–Fe bond of **8** is mostly stabilised by strong σ-donation from **8** having six times weaker π-back-donation from $Fe(CO)_4$ to backbone of **1** (see Table 4). The corresponding dissociation energy is 35.69 kcal mol⁻¹ **1** likely to form a week bond with the nickel–carbonyl.
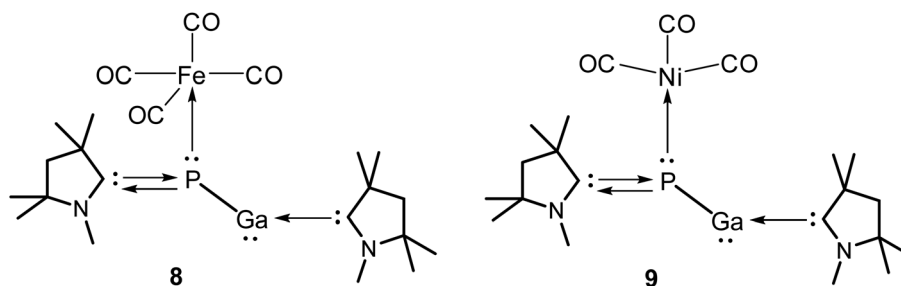

Fig. 6 Metal-carbonyl $(cAAC)_2PGa$-$M(CO)_n$ [M = Fe (**8**), n = 4; Ni (**9**), n = 3] of $(cAAC)_2PGa$ (**1**).
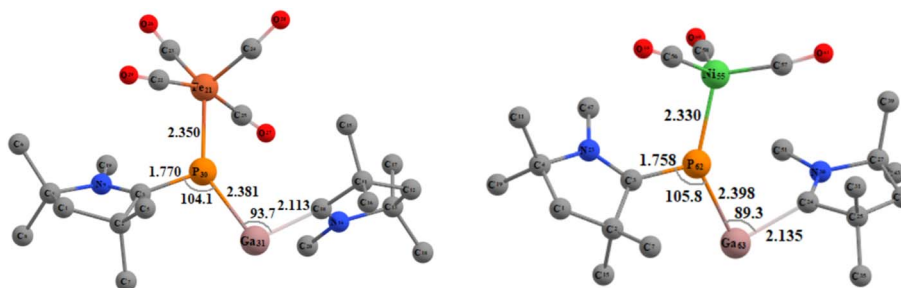

Fig. 7 Optimized geometries of compound **8** (left) and **9** (right) in singlet ground state at BP86-D3(BJ)/def2-TZVPP level of theory.

Table 4 The EDA-NOCV results of $(cAAC)_2GaP$–$M(CO)_n$ bond of $(cAAC)_2GaP$–$M(CO)_n$ complex [M = Fe, n = 4 (**8**); M = Ni, n = 3 (**9**)] using $[(cAAC)_2GaP]$ and $[M(CO)_n]$ in the electronic singlet (S) states as interacting fragments at the M06-2X/TZ2P level of theory. Energies are in kcal mol⁻¹

Energy	Interaction	$(cAAC)_2PGa$ (S) + $Fe(CO)_4$ (S)	$(cAAC)_2PGa$ (S) + $Ni(CO)_3$ (S)
Complex		**8**	**9**
ΔE_{int}		−43.9	−30.0
ΔE_{Pauli}		88.2	64.6
$\Delta E_{disp}{}^a$		−1.7 (1.1%)	−1.5 (1.4%)
$\Delta E_{elstat}{}^a$		−84.3 (56.7%)	−64.6 (59.6%)
$\Delta E_{orb}{}^a$		−62.6 (42.1%)	−42.3 (39.0%)
$\Delta E_{orb(1)}{}^b$	$(cAAC)_2GaP \rightarrow M(CO)_n$ σ-donation	−42.3 (66.6%)	−29.4 (69.5%)
$\Delta E_{orb(2)}{}^b$	$(cAAC)_2GaP \leftarrow M(CO)_n$ π-backdonation	−5.8 (9.3%)	−3.5 (8.3%)
$\Delta E_{orb(rest)}$		−14.5 (23.1%)	−9.4 (22.2%)

^{a} The values in the parentheses show the contribution to the total attractive interaction $\Delta E_{disp} + \Delta E_{elstat} + \Delta E_{orb}$. ^{b} The values in parentheses show the contribution to the total orbital interaction ΔE_{orb}.
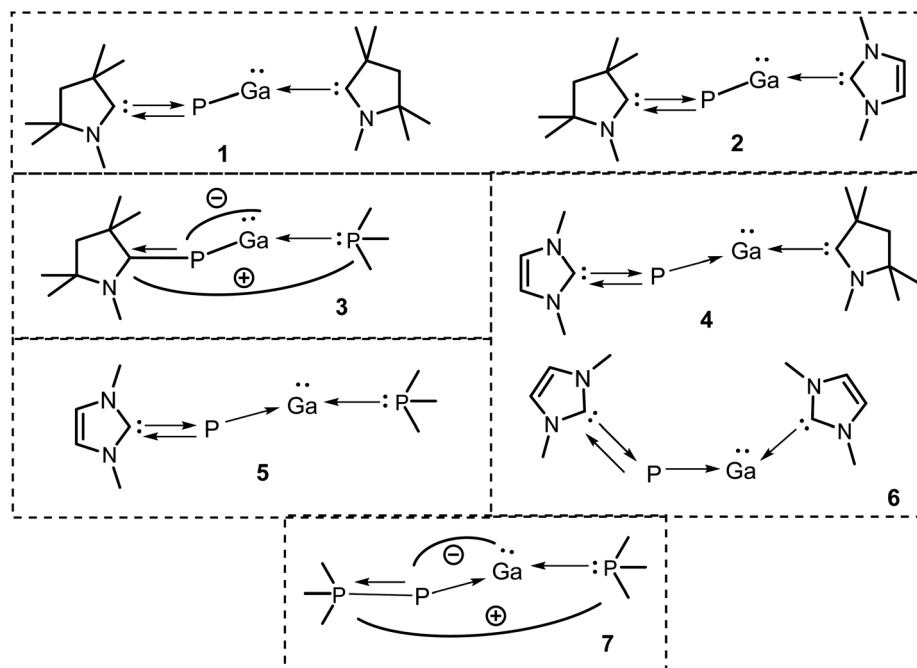
Scheme 3 Overall bonding scenarios of compounds 1–7.

Conclusion

In conclusion, the stability and bonding of monomeric GaP with donor base ligands have been studied with three different functionals [GGA, BP86; hybrid, B3LYP; GGA and *meta*-GGA, M06-2X]. We will prefer M06-2X functional over other two functionals. A similar problem previously faced by Frenking *et al.* They have shown that M06 functional is more suitable providing support with additional calculations with CCSD(T)/MP2 level of theory which are believed to be the gold standard. Using various donor-base ligands, including cAAC, NHC, and PMe_3, we have examined the structure and bonding of gallium phosphide. Due to the better σ-donation and π-acceptance properties of cAAC, it is observed that the bond between cAAC and P (1–3) has a partial double bond character. The larger and diffused orbitals of Ga and the poor π-acceptance of the donor-base ligands, NHC and PMe_3 made the Ga–L′ bond weaker. EDA-NOCV studies predicted the best bonding between ligand fragments and PGa moiety is dative due to the interaction of neutral singlet fragments. For the compounds 1–2, and 4–6. Whereas, for 3, and 7 the best bonding scenario was when the singly charged doublet $[L,L′]^+$ and $[PGa]^-$ fragments interacted to form electron sharing and dative bonds (Scheme 3). EDA-NOCV studies conducted on P–Ga bond suggested that 1 and 2 will be electron sharing between the interaction of neutral doublet fragments of [LP] and [GaL′]. The bond between P–Ga is dative for 3–7 happening due to the interaction of singly charged singlet fragments of $[LP]^-$ and $[GaL′]^-$. The bond dissociation energies (−120 to −125 kcal mol^{-1} with M06-2X functional) of [L,L′] and GaP pair are significantly high for 1 [L = cAAC, L′ = cAAC] and 2 [L = cAAC, L′ = NHC] suggesting that they may be possible to experimentally isolate in the

laboratory. Further calculations have showed that cAAC stabilised PGa compound can form stable complex with iron-carbonyl.

Conflicts of interest

The authors do not have any conflict of interest.

Acknowledgements

References

1 Z.-C. Zhang and D.-L. Cui, *Chin. J. Chem.*, 2005, **23**, 1213–1217.
2 A. Höglund, C. W. M. Castleton and S. Mirbt, *Phys. Rev. B: Condens. Matter Mater. Phys.*, 2005, **72**, 195213–195216.
3 J. Mašek, J. Kudrnovský, F. Máca, J. Sinova, A. H. MacDonald, R. P. Campion, B. L. Gallagher and T. Jungwirth, *Phys. Rev. B: Condens. Matter Mater. Phys.*, 2007, **75**, 045202–045207.
4 C. Çelebi, P. M. Koenraad, A. Yu. Silov, W. Van Roy, A. M. Monakhov, J.-M. Tang and M. E. Flatté, *Phys. Rev. B: Condens. Matter Mater. Phys.*, 2008, **77**, 075328–075335.
5 P. Karamanis, C. Pouchan and J. Leszczynski, *J. Phys. Chem. A*, 2008, **112**, 13662–13671.
6 Z.-C. Zhang and B.-P. Wang, *Part. Part. Syst. Charact.*, 2009, **26**, 53–57.
7 A. Y. Timoshkin and H. F. Schaefer, *J. Phys. Chem. A*, 2010, **114**, 516–525.

8 F. Cheng, K. George, A. L. Hector, M. Jura, A. Kroner, W. Levason, J. Nesbitt, G. Reid, D. C. Smith and J. W. Wilson, *Chem. Mater.*, 2011, **23**, 5217–5222.

9 O. Romanyuk, T. Hannappel and F. Grosse, *Phys. Rev. B: Condens. Matter Mater. Phys.*, 2013, **88**, 115312–115320.

10 C. Lacroix, S. Lambert-Milot, R. A. Masut, P. Desjardins and D. Ménard, *Phys. Rev. B: Condens. Matter Mater. Phys.*, 2013, **87**, 024412–024422.

11 J. R. Chelikowsky and M. L. Cohen, *Phys. Rev. B: Solid State*, 1973, **14**, 556–582.

12 R. L. Wells and W. L. Gladfelter, *J. Cluster Sci.*, 1997, **8**, 217–238.

13 S. Schulz, *Adv. Organomet. Chem.*, 2003, **49**, 225–317.

14 M. A. Malik, M. Afzaal and P. O'Brien, *Chem. Rev.*, 2010, **110**, 4417–4446.

15 (*a*) F. P. Miller, A. F. Vandome and J. McBrewster, *Gallium Arsenide Phosphide*, Alphascript, Publishing, India, 2010; (*b*) P. B. Hart, Gallium Phosphide, in *Electronics Design Materials*, ed. W. F. Waller, Macmillan Engineering Evaluations, Palgrave Macmillan, London, 1971; (*c*) F. P. Miller, A. F. Vandome and J. McBrewster, *Aluminium Gallium Phosphide*, Alphascript Publishing, India, 2010; (*d*) S. Singh and P. Srivastava, *Appl. Nanosci.*, 2012, **3**, 89–94; (*e*) T. Zhang, Y. Qian, H. Gao, Z.-C. Huang-Fu, J. B. Brown and Y. Rao, *J. Phys. Chem. C*, 2022, **126**, 6761–6772.

16 E. D. Palik, *Handbook of Optical Constants of Solids*, Elsevier, Burlington, 1985.

17 E. D. Palik, *Handbook of Optical Constants of Solids*, Burlington Elsevier Science & Technology Ann Arbor, Michigan Proquest, 1991, vol. 2.

18 M. J. Weber, *Handbook of Optical Materials*, Crc Press, Boca Raton, 2003.

19 J. Václavík and D. Vápenka, in *EPJ Web of Conferences*, 2013, 48, p. 0028.

20 W. E. Dasent, *Nonexistent Compounds: Compounds of Low Stability*, Dekker, New York, 1966.

21 D. W. N. Wilson, J. Feld and J. M. Goicoechea, *Angew. Chem., Int. Ed.*, 2020, **59**, 20914–20918.

22 M. K. Sharma, C. Wölper, G. Haberhauer and S. Schulz, *Angew. Chem., Int. Ed.*, 2021, **60**, 6784–6790.

23 D. W. N. Wilson, W. K. Myers and J. M. Goicoechea, *Dalton Trans.*, 2020, **49**, 15249–15255.

24 J. Feld, D. W. N. Wilson and J. M. Goicoechea, *Angew. Chem., Int. Ed.*, 2021, **60**, 22057–22061.

25 M. K. Sharma, C. Wölper, G. Haberhauer and S. Schulz, *Angew. Chem., Int. Ed.*, 2021, **60**, 21784–21788.

26 J. Krüger, C. Wölper and S. Schulz, *Angew. Chem., Int. Ed.*, 2020, **60**, 3572–3575.

27 B. Li, C. Wölper, G. Haberhauer and S. Schulz, *Angew. Chem., Int. Ed.*, 2020, **60**, 1986–1991.

28 (*a*) T. I. Demirer, B. Morgenstern and D. M. Andrada, *Eur. J. Inorg. Chem.*, 2022, DOI: 10.1002/ejic.202200477; (*b*) T. J. Dudley, W. W. Brown and M. R. Hoffmann, *J. Phys. Chem. A*, 1999, **103**, 5152–5160.

29 J.-S. Lu, M.-C. Yang and M.-D. Su, *J. Phys. Chem. A*, 2017, **121**, 6630–6637.

30 (*a*) K. Morokuma, *J. Chem. Phys.*, 1971, **55**, 1236–1244; (*b*) T. Ziegler and A. Rauk, *Theor. Chim. Acta*, 1977, **46**, 1–10; (*c*) M. Mitoraj and A. Michalak, *Organometallics*, 2007, **26**, 6576–6580; (*d*) M. Mitoraj and A. Michalak, *J. Mol. Model.*, 2008, **14**, 681–687; (*e*) G. te Velde, F. M. Bickelhaupt, E. J. Baerends, C. Fonseca Guerra, S. J. A. van Gisbergen, J. G. Snijders and T. Ziegler, *J. Comput. Chem.*, 2001, **22**, 931–967.

31 (*a*) G. Deng, S. Pan, G. Wang, L. Zhao, M. Zhou and G. Frenking, *Angew. Chem.*, 2020, **132**, 10690–10696; (*b*) D. M. Andrada and G. Frenking, *Angew. Chem., Int. Ed.*, 2015, **54**, 12319–12324; (*c*) S. K. Kushvaha, S. M. N. V. T. Gorantla and K. C. Mondal, *J. Phys. Chem. A*, 2022, **126**, 845–858; (*d*) M. Hermann, C. Goedecke, C. Jones and G. Frenking, *Organometallics*, 2013, **32**, 6666–6673; (*e*) S. M. N. V. T. Gorantla, S. Pan, K. C. Mondal and G. Frenking, *Chem. – Eur. J.*, 2020, **26**, 14211–14220; (*f*) L.-H. Mou, Y. Li, Z.-Y. Li, Q.-Y. Liu, H. Chen and S.-G. He, *J. Am. Chem. Soc.*, 2021, **143**, 19224–19231; (*g*) L. Bondì, A. L. Garden, P. Jerabek, F. Totti and S. Brooker, *Chem. – Eur. J.*, 2020, **26**, 13677–13685; (*h*) S. M. N. V. T. Gorantla and K. C. Mondal, *Eur. J. Inorg. Chem.*, 2021, **2021**, 960–968; (*i*) F. S. S. Schneider, G. F. Caramori, R. L. T. Parreira, V. Lippolis, M. Arca and G. Ciancaleoni, *Eur. J. Inorg. Chem.*, 2018, **2018**, 1007–1015; (*j*) I. Rodstein, L. Kelling, J. Löffler, T. Scherpf, A. Sarbajna, D. M. Andrada and V. H. Gessner, *Chem. Sci.*, 2022, **13**, 13552–13562; (*k*) S. M. N. V. T. Gorantla, M. Francis, S. Roy and K. C. Mondal, *RSC Adv.*, 2021, **11**, 6586–6603.

32 E. Nag, M. Francis, S. Battuluri, B. B. Sinu and S. Roy, *Chem. – Eur. J.*, 2022, e202201242.

33 (*a*) S. Roy, K. C. Mondal and H. W. Roesky, *Acc. Chem. Res.*, 2016, **49**, 357–369; (*b*) K. C. Mondal, S. Roy and H. W. Roesky, *Chem. Soc. Rev.*, 2016, **45**, 1080–1111; (*c*) H. Braunschweig, R. D. Dewhurst and V. H. Gessner, *Chem. Soc. Rev.*, 2013, **42**, 3197–3208; (*d*) M.-A. Légaré, C. Pranckevicius and H. Braunschweig, *Chem. Rev.*, 2019, **119**, 8231–8261; (*e*) M. Melaimi, R. Jazzar, M. Soleilhavoup and G. Bertrand, *Angew. Chem., Int. Ed.*, 2017, **56**, 10046–10068.

34 R. Kinjo, B. Donnadieu and G. Bertrand, *Angew. Chem., Int. Ed.*, 2010, **49**, 5930–5933.

35 V. Lavallo, Y. Canac, C. Präsang, B. Donnadieu and G. Bertrand, *Angew. Chem., Int. Ed.*, 2005, **44**, 5705–5709.

36 D. Pichon, M. Soleilhavoup, J. Morvan, G. P. Junor, T. Vives, C. Crévisy, V. Lavallo, J.-M. Campagne, M. Mauduit, R. Jazzar and G. Bertrand, *Chem. Sci.*, 2019, **10**, 7807–7811.

37 (*a*) A. D. Becke, *Phys. Rev. A: At., Mol., Opt. Phys.*, 1988, **38**, 3098–3100; (*b*) J. P. Perdew, *Phys. Rev. B: Condens. Matter Mater. Phys.*, 1986, **33**, 8822–8824.

38 C. Lee, W. Yang and R. G. Parr, *Phys. Rev. B: Condens. Matter Mater. Phys.*, 1988, **37**, 785–789.

39 Y. Zhao and D. G. Truhlar, *Theor. Chem. Acc.*, 2008, **120**, 215–241.

40 M. J. Frisch, *et al.*, *Gaussian 16, Revision A.03*, Gaussian, Inc., Wallingford CT, 2016.

41 K. B. Wiberg, *Tetrahedron*, 1968, **24**, 1083–1096.

42 (a) F. Weinhold and C. Landis, *Valency and Bonding, A Natural Bond Orbital Donor-Acceptor Perspective*, Cambridge University Press, Cambridge, 2005; (b) C. R. Landis and F. Weinhold, The NBO View of Chemical Bonding, *The Chemical Bond: Fundamental Aspects of Chemical Bonding*, ed. G. Frenking and S. Shaik, Wiley, 2014, pp. 91–120; (c) A. E. Reed, L. A. Curtiss and F. Weinhold, *Chem. Rev.*, 1988, **88**, 899–926.

43 T. A. Keith, *AIMAll (Version 10.05.04)*, 2010, **https://aim.tkgristmill.com**.

44 M. A. Celik, R. Sure, S. Klein, R. Kinjo, G. Bertrand and G. Frenking, *Chem. – Eur. J.*, 2012, **18**, 5676–5692.

45 S. Roy, K. C. Mondal, S. Kundu, B. Li, C. J. Schürmann, S. Dutta, D. Koley, R. Herbst-Irmer, D. Stalke and H. W. Roesky, *Chem. – Eur. J.*, 2017, **23**, 12153–12157.

46 Y. Wang, Y. Xie, P. Wei, R. B. King, H. F. Schaefer, P. v. R. Schleyer and G. H. Robinson, *J. Am. Chem. Soc.*, 2008, **130**, 14970–14971.

47 L. Weber, *Eur. J. Inorg. Chem.*, 2000, **2000**, 2425–2441.

48 M. M. Siddiqui, S. Banerjee, S. Bose, S. K. Sarkar, S. K. Gupta, J. Kretsch, N. Graw, R. Herbst-Irmer, D. Stalke, S. Dutta, D. Koley and H. W. Roesky, *Inorg. Chem.*, 2020, **59**, 11253–11258.

49 M. Kapitein and C. von Hänisch, *Eur. J. Inorg. Chem.*, 2015, **2015**, 837–844.

50 M. Kapitein, M. Balmer, L. Niemeier and C. von Hänisch, *Dalton Trans.*, 2016, **45**, 6275–6281.

51 A. Kuczkowski, S. Schulz and M. Nieger, *Appl. Organomet. Chem.*, 2004, **18**, 244–251.

52 (a) R. F. Bader, *Atoms in Molecules: A Quantum Theory*, Clarendon Pr, Oxford, 1990; (b) R. F. W. Bader, *Chem. Rev.*, 1991, **91**, 893–928; (c) R. F. W. Bader, *Acc. Chem. Res.*, 1985, **18**, 9–15; (d) C. F. Matta and R. J. Boyd, *The Quantum Theory of Atoms in Molecules: From Solid State to DNA and Drug Design*, Wiley-Vch, Weinheim, 2007.